

Chaotic and Regular Dynamics In the Three-site Bose-Hubbard Model

A. A. Bychek¹, P. S. Muraev^{1,2}, D. N. Maksimov^{1,2,3}, and A. R. Kolovsky^{1,2}

¹*Kirensky Institute of Physics, Federal Research Center KSC SB RAS, 660036, Krasnoyarsk, Russia*

²*Siberian Federal University, 660041, Krasnoyarsk, Russia*

³*Reshetnev Siberian State University of Science and Technology, 660037, Krasnoyarsk, Russia*

(Dated: October 29, 2019)

We analyze the energy spectrum of the three-site Bose-Hubbard model. It is shown that this spectrum is a mixture of the regular and irregular spectra associated with the regular and chaotic components of the classical Bose-Hubbard model. We find relative volumes of these components by using the pseudoclassical approach. Substituting these values in the Berry-Robnik distribution for the level spacing statistics we obtain good agreement with the numerical data.

I. INTRODUCTION

The Bose-Hubbard (BH) model contains the basic physics of interacting bosons in a lattice [1] with particular interest in the context of cold Bose atoms in optical lattices [2]. The many-site BH model is known to belong to the class of quantum nonintegrable systems whose spectral and dynamical features are consistent with predictions of the theory of Quantum chaos [3]. The chaotic dynamics of cold Bose atoms in the optical lattice has been intensively studied in recent years [3–9]. On the contrary, the two-site BH model is completely integrable, i.e. can be solved analytically [10]. The cold atom realizations of the two-site BH model are nowadays a popular playground for studying such phenomena as Josephson oscillations and self-trapping [11, 12].

In this work we analyze the three-site BH model which is the simplest representative of the nonintegrable BH Hamiltonians. On the other hand, the three-site system retains certain features of the integrable two-site system [4, 13, 14]. For example, it can show the generalized Josephson oscillations with quasiperiodic change of the site occupations [4]. In the work we give description of dynamical regimes of the three-site BH model and identify their signatures in the energy spectrum. There are several ways to distinguish regular and chaotic regimes: Loschmidt echo [15, 16], machine learning algorithms [17], and semiclassical (or, better to say, pseudoclassical) methods [6, 18]. Here we employ the latter approach – we introduce the classical analogue of the quantum three-site BH model and demonstrate that it shows a mixture of chaotic and regular dynamics. We quantify chaos by calculating the finite-time Lyapunov exponent and relative volumes of the regular and chaotic components.

II. THE SYSTEM

The Bose-Hubbard Hamiltonian reads

$$\hat{\mathcal{H}} = -\frac{J}{2} \sum_{l=1}^{\bar{L}} \left(\hat{a}_{l+1}^\dagger \hat{a}_l + h.c. \right) + \frac{U}{2} \sum_l \hat{a}_l^\dagger \hat{a}_l^\dagger \hat{a}_l \hat{a}_l, \quad (1)$$

where the index l labels the l th well of the optical potential, \hat{a}_l and \hat{a}_l^\dagger are the bosonic annihilation and creation operators,

$$[\hat{a}_l, \hat{a}_l^\dagger] = \hbar \delta_{l,l'}, \quad (2)$$

J is the hopping matrix element, and U the microscopic interaction constant. Experimentally, the three-well optical potential can be realized using different technics [19] where the hopping energy and the particle interaction can be controlled separately.

Depending on the lattice geometry of the summation limit in the hopping term \bar{L} can take two different values. If the potential wells are arranged along a straight line the system is a linear oligomer (LO) where the hopping terminated at the first $l = 1$ and the last $l = L$ sites on the line. Then we have

$$\bar{L}_{LO} = L - 1. \quad (3)$$

Another geometry is a circular oligomer (CO) where we additionally have the hopping between the first and last sites that leads to the periodical boundary condition $\hat{a}_{L+1} = \hat{a}_1$. Then

$$\bar{L}_{CO} = L. \quad (4)$$

The periodic boundary condition also implies conservation of the total quasimomentum. This can be proved by rewriting the Hamiltonian (1) in terms of the operators \hat{b}_k and \hat{b}_k^\dagger ,

$$\hat{b}_k = \frac{1}{\sqrt{L}} \sum_l \exp(i2\pi kl/L) \hat{a}_l. \quad (5)$$

which annihilate and create a particle in the Bloch state with the quasimomentum $\kappa = 2\pi k/L$. We obtain

$$\hat{\mathcal{H}} = -J \sum_{k=-1,0,1} \cos\left(\frac{2\pi k}{3}\right) \hat{b}_k^\dagger \hat{b}_k + \frac{U}{6} \sum_{k_1, k_2, k_3, k_4} \hat{b}_{k_1}^\dagger \hat{b}_{k_2}^\dagger \hat{b}_{k_3} \hat{b}_{k_4} \tilde{\delta}(k_1 + k_2 - k_3 - k_4), \quad (6)$$

where the presence of the δ -function in the interaction term insures that the total quasimomentum is conserved. The Hilbert space of (6) is spanned by the quasimomentum Fock states $|n_{-1}, n_0, n_{+1}\rangle$, where $\sum_k n_k = N$ is the total number of particles.

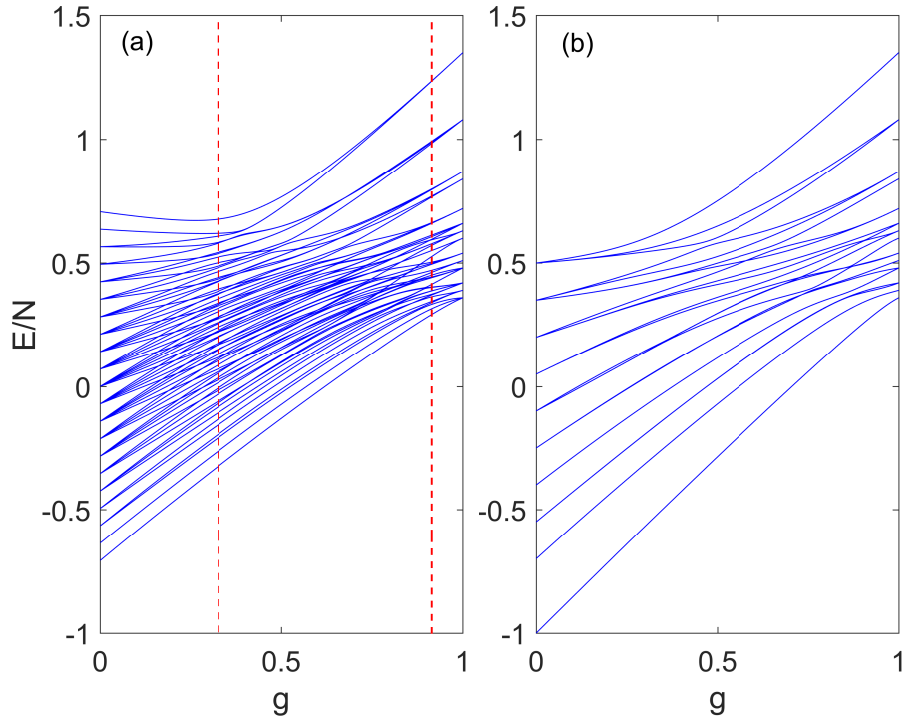


FIG. 1: Energy spectrum of $N = 10$ bosons as a function of the macroscopic interaction constant $g = UN/3$ and the hopping matrix element $J = 1 - g$. Left panel: the whole spectrum of the linear oligomer (LO). Right panel: the spectrum of the circular oligomer (CO) for the independent subset of states with zero total quasimomentum.

Next we discuss the energy spectrum of the system. Fig. 1 shows the energy spectrum for LO (left panel) and CO (right panel) as a function of the macroscopic interaction constant $g = UN/3$, where we simultaneously set the hopping matrix element to $J = 1 - g$. This allows us to consider the both cases of weak and strong coupling/interaction – the case of $g = 0$ corresponds to the system of noninteracting bosons whereas in the case of $g = 1$ the interwell tunnelling is completely suppressed. In these limits the BH model is integrable and its energy spectrum can be found analytically. However, within the intermediate range of g it is highly irregular and the energy levels exhibit avoided crossings as they approach each other, see the area between two dashed red lines in Fig. 1(a). In this parameter region the system is nonintegrable. Following the standard procedure we calculate the normalized distances between the nearest levels $s = (E_{n+1} - E_n)\rho(E_n)$ where $\rho(E)$ is the density of states, see Fig. 2(a). In Fig. 2(b) we show the integrated level spacing distribution $I(s) = \int_0^s ds' P(s')$ for the central energy region comprising 70 percent of the states (solid line) and compare it with the Poisson distribution (dash-dotted line),

$$P_P(s) = \exp(-s), \quad (7)$$

and the Wigner-Dyson distribution (dashed line),

$$P_{WD}(s) = \frac{\pi}{2} s \exp(-\frac{\pi}{4} s^2). \quad (8)$$

It is seen that the level spacing statistics is close to the Wigner-Dyson distribution which is a hallmark of Quantum chaos.

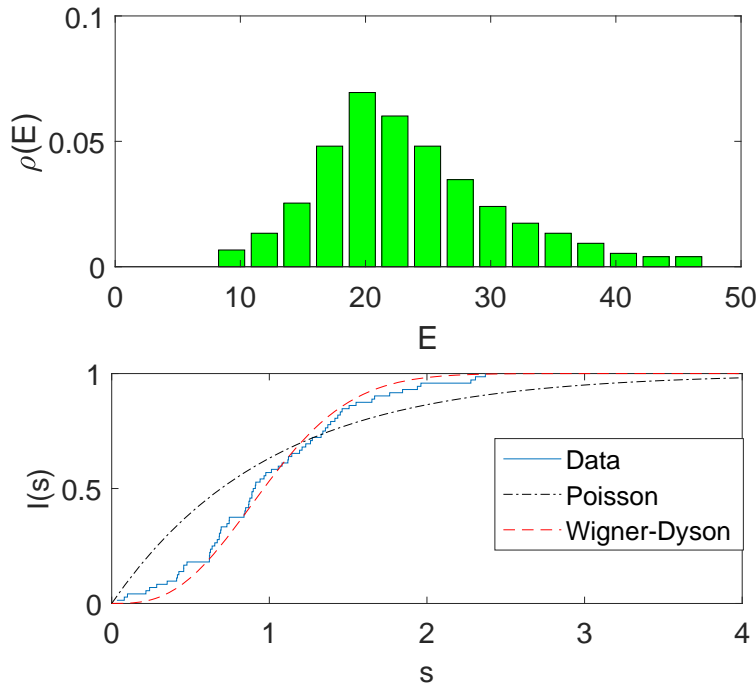


FIG. 2: Upper panel: The density of states ρ of the three-site Bose-Hubbard model. Lower panel: Integrated distribution $I(s) = \int_0^s ds' P(s')$ for the Poisson level spacing statistics $P_P(s)$ (dash-dotted black curve), the Wigner-Dyson statistics $P_{WD}(s)$ (dashed red curve), and numerical data $P(s)$ (blue) for the central part of the energy spectrum. Parameters are $N = 30$, $g = 0.8$, and $J = 1 - g$.

We stress that we get a reasonable agreement with the Wigner-Dyson statistics only because we neglect 30 percent of the energy levels which are presumably not chaotic. A more accurate description of the spectrum is given by the Berry-Robnic distribution,

$$P_{BR}(s) = \left[\nu_r^2 \operatorname{erfc}\left(\frac{\sqrt{\pi}}{2} \nu_c s\right) + (2\nu_r \nu_c + \frac{\pi}{2} \nu_c^2 s) \exp(-\frac{\pi}{4} \nu_c^2 s^2) \right] \exp(-\nu_r s), \quad (9)$$

which includes the relative size of the regular (ν_r) and chaotic (ν_c) components as the fitting parameters. In the next section we obtain these fitting parameters from the first principles by using the pseudoclassical approach.

III. REGULAR AND CHAOTIC DYNAMICS

Pseudoclassical approach borrows its ideas from the semiclassical method in single-particle quantum mechanics to address the spectral and dynamical properties of the system of N interacting bosons with $1/N$ playing the role of Planck's constant[6, 18, 20, 21]. In this approach the operators are substituted by their Weyl images which gives

$$\frac{\hat{a}_l}{\sqrt{N}} \rightarrow a_l, \quad \frac{\hat{a}_l^\dagger}{\sqrt{N}} \rightarrow a_l^*, \quad (10)$$

and

$$\frac{\hat{H}}{N} \rightarrow H = -\frac{J}{2} \sum_{l=1}^{\bar{L}} (a_{l+1}^* a_l + c.c.) + \frac{g}{2} \sum_{l=1}^L |a_l|^4 \quad (11)$$

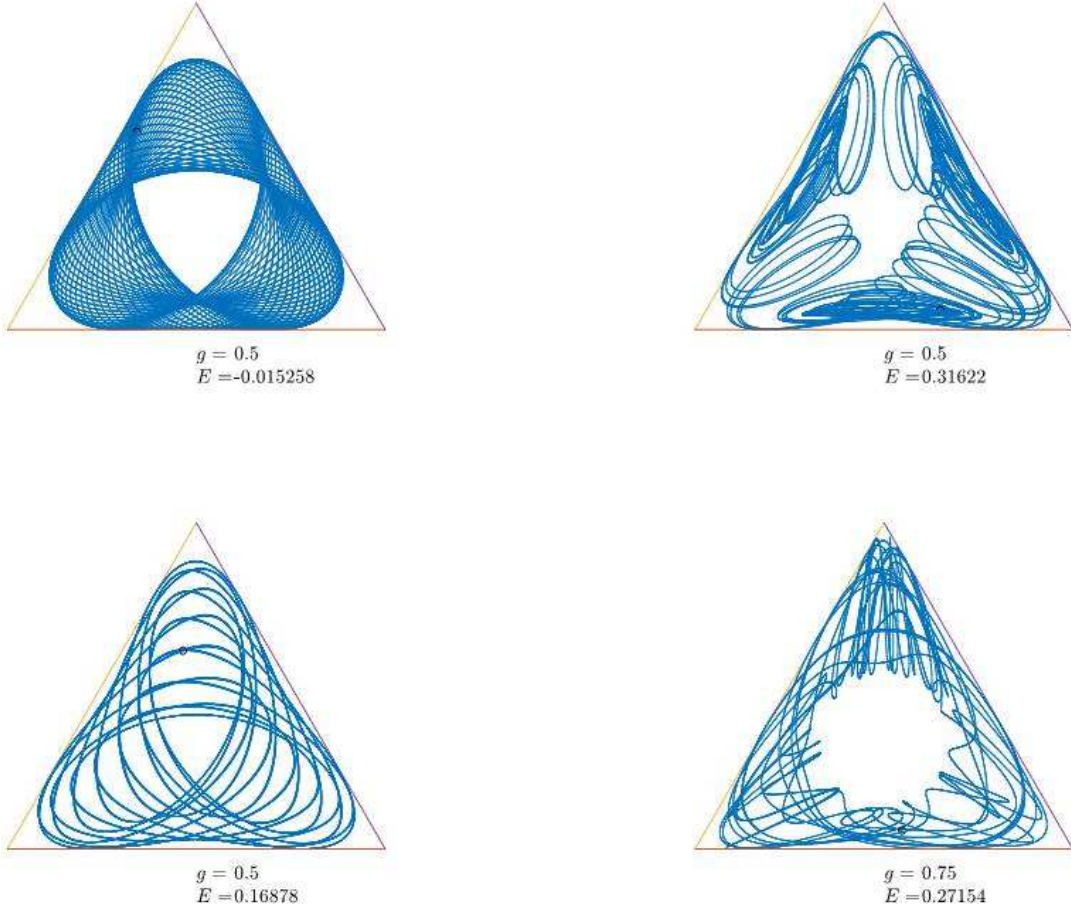


FIG. 3: Examples of regular (a) and chaotic (b) trajectories. Regular dynamics correspond to the Josephson oscillations of the site occupations.

where $g = UN/L$ is the macroscopic interaction constant. In the semiclassical limit $N \rightarrow \infty$ and $U = g/N \rightarrow 0$ this approach is equivalent to the mean-field approximation. The main advantage of the pseudoclassical approach above the mean-field approximation is that it can treat the case of finite N as well. The validity of this approach was discussed, for example, in Ref. [18] where it was demonstrated that it works well till $N \sim 10$. In what follows, however, we shall assume the limit $N \rightarrow \infty$ where the Hamiltonian (11) generates the Hamilton equations of motion

$$i \frac{da_l}{dt} = \frac{\partial H}{\partial a_l^*} = -\frac{J}{2} (a_{l-1} + a_{l+1}) + g|a_l|^2 a_l, \quad i \frac{da_l^*}{dt} = -\frac{\partial H}{\partial a_l}, \quad (12)$$

which are known as the discrete nonlinear Schrödinger equation (DNLSE) [22]. The solution $a_l(t)$ is the classical trajectory and, since $|a_1(t)|^2 + |a_2(t)|^2 + |a_3(t)|^2 = 1$, it is bounded to the S^5 sphere in the 6-dimensional phase space.

We numerically solve Hamilton's equations of motion (12) for the ensemble of initial conditions uniformly distributed over the whole phase space, i.e., over the surface of the sphere S^5 . As an example, Fig. 3 samples regular and chaotic trajectories from this ensemble. We distinguish between regular and chaotic trajectories by calculating the finite-time Lyapunov exponent defined according to the following equation [23–25]

$$\lambda(t) = \frac{|\delta \mathbf{a}(t)|}{|\delta \mathbf{a}_0|} / t. \quad (13)$$

Here $\delta \mathbf{a} = (\delta a_1, \delta a_2, \delta a_3, \delta a_1^*, \delta a_2^*, \delta a_3^*)^T$ is the deviation from a given trajectory $\mathbf{a}(t)$ which obeys the linearized equation of motion

$$i \frac{d}{dt} \delta \mathbf{a} = M[\mathbf{a}(t)] \delta \mathbf{a}, \quad (14)$$

with $M[\mathbf{a}(t)]$ being $2L \times 2L$ matrix of the following structure:

$$M[\mathbf{a}(t)] = \begin{pmatrix} A + gB & gC \\ -gC^* & -(A + gB)^* \end{pmatrix}, \quad (15)$$

$$A_{l,m} = -\frac{J}{2}(\delta_{l+1,m} + \delta_{l-1,m}), \quad (16)$$

$$B_{l,m} = (2|a_l(t)|^2 - \frac{E}{g})\delta_{l,m} \quad C_{l,m} = a_l^2(t)\delta_{l,m} \quad (17)$$

$$E = \frac{1}{3}g - J \cos(\frac{2\pi}{3}k) \quad (18)$$

The finite-time Lyapunov exponent shows the temporary evolution of the separation between two close initial conditions and for sufficiently long computational times converges to the celebrated Lyapunov exponent. Namely, it approaches zero for regular trajectories ($\lambda \simeq 0$) while it is always well above zero for chaotic trajectories ($\lambda \geq 0$), see Fig. 4(a).

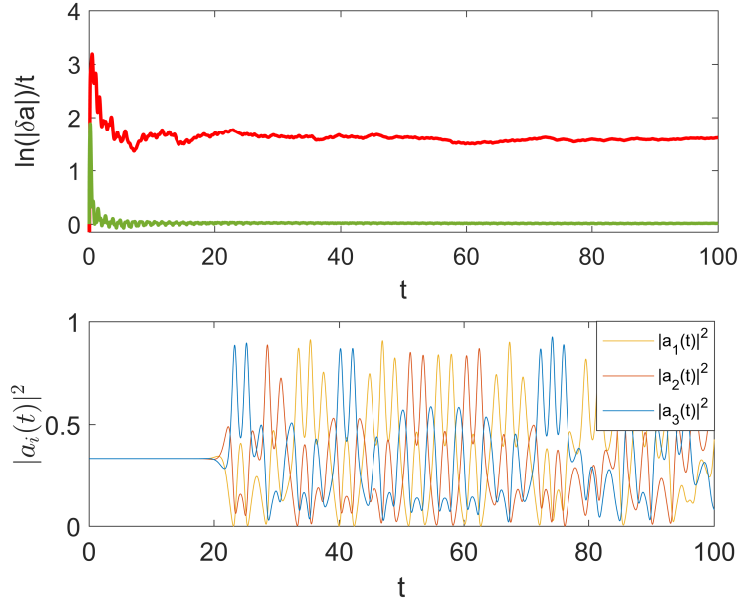


FIG. 4: Upper panel: Finite-time Lyapunov exponent $\lambda(t)$ for regular ($\lambda \simeq 0|_{t=t_{end}}$) and chaotic ($\lambda > 0|_{t=t_{end}}$) trajectories. Lower panel: The phenomenon of the dynamical or modulation instability for the Bloch wave with nonzero total quasimomentum due to chaoticity.

Next, we calculate the exponent λ for all trajectories from the uniform ensemble of initial conditions. The insets in Fig. 5 show λ as a function of the trajectory energy E (which is obviously a conserved quantity). Additional vertical lines mark the energies of the nonlinear Bloch waves,

$$a_l(t) = \frac{1}{\sqrt{L}} \exp[i\kappa l + iJ \cos(\kappa)t - i g t], \quad \kappa = 2\pi k/L, \quad (19)$$

which are stable ($|\kappa| < \pi/2$) or unstable ($|\kappa| > \pi/2$) periodic trajectories of the system, see Fig. 4(b). We count the number of regular and chaotic trajectories by introducing some $\lambda_{cr} \ll 1$ which we set in our simulations to $\lambda_{cr} = 0.01$. Then all trajectories with finite-time Lyapunov exponent $\lambda < \lambda_{cr}$ are treated as regular. Following this idea we find volumes of the regular and chaotic components as the relative number of regular and chaotic trajectories. The results are shown in the main panel in Fig. 5 where the blue curve refers to the case of circular oligomer and the red curve to the linear oligomer.

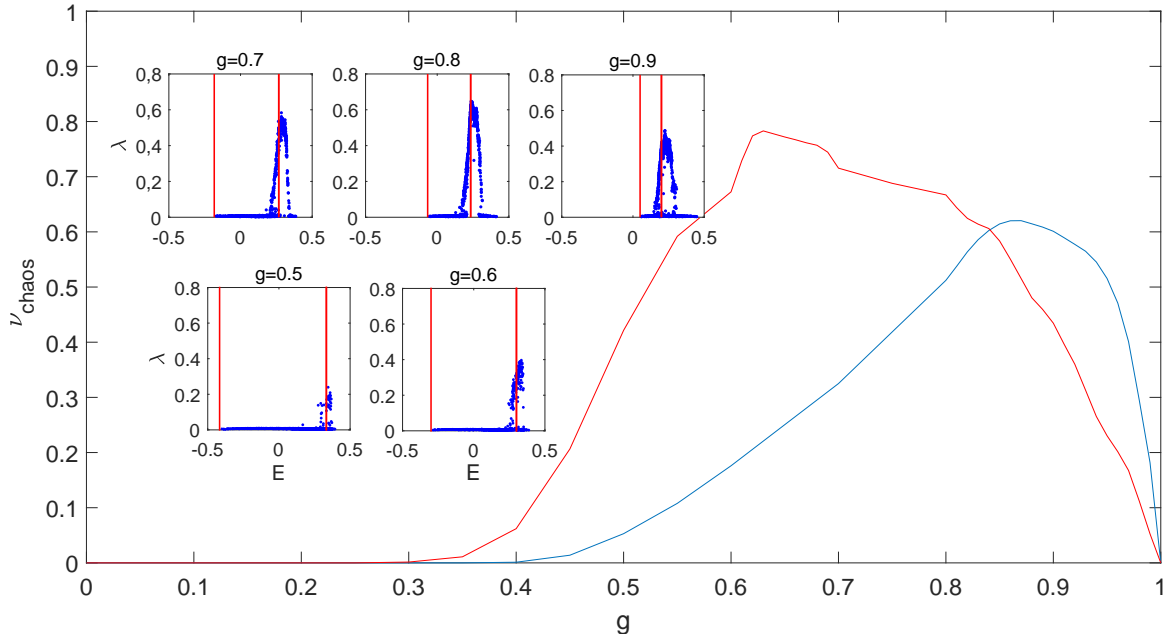


FIG. 5: The volume of the chaotic component as a function of the macroscopic interaction constant g for the linear oligomer (red curve) and circular oligomer (blue curve). Results are based on the numerical analysis of the ensemble of 500 trajectories with initial conditions uniformly distributed over the whole phase space. Insets show the Lyapunov exponent for each trajectory from the uniform ensemble as a function of the trajectory energy given by Eq. (11). Vertical lines mark energies of the periodic trajectories (19).

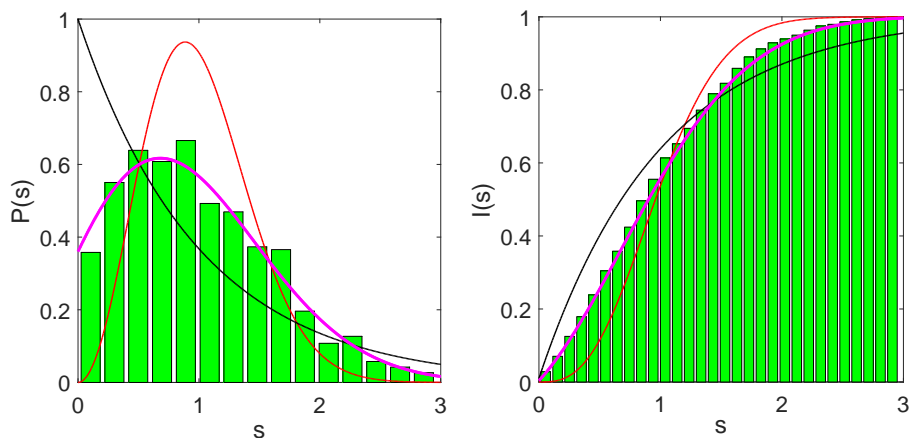


FIG. 6: The level spacing distribution (left panel) and integrated level spacing distribution (right panel) of the quantum energy spectrum in the comparison with the Berry-Robin distribution (magenta line) with v_r and v_c extracted from results of the pseudoclassical analysis. Additionally, the red and black lines show the Wigner-Dyson and Poisson distribution. Parameters: linear oligomer, $v_c = 0.8$, $v_r = 0.2$, $N = 50$, $g = 0.8$, $J = 1 - g$.

IV. RESULTS AND CONCLUSIONS

Now we are prepared to discuss the statistical properties of the whole energy spectrum of the three-site BH system. The histograms in Fig. 6 show the level spacing distribution and integrated level spacing distribution as compared to the Berry-Robnic distribution (9) which is depicted by the magenta line. In the distribution (9) we use the values of the parameters v_c and v_r obtained in the previous section. A nice agreement is noticed. This agreement proves that the three-site BH model is a genuine mixed system where the regular spectrum coexists with the irregular spectrum. Furthermore, the results presented in the insets in Fig. 5 undoubtedly tell us which part of the energy spectrum is associated with the chaotic dynamics and, hence, is irregular.

ACKNOWLEDGMENTS

This work has been supported through Russian Science Foundation Grant N19-12-00167.

-
- [1] HA Gersch and GC Knollman, “Quantum cell model for bosons,” *Physical Review* **129**, 959 (1963).
 - [2] Dieter Jaksch, Christoph Bruder, Juan Ignacio Cirac, Crispin W Gardiner, and Peter Zoller, “Cold bosonic atoms in optical lattices,” *Physical Review Letters* **81**, 3108 (1998).
 - [3] Andrey R. Kolovsky, “Bose–hubbard hamiltonian: Quantum chaos approach,” *International Journal of Modern Physics B* **30**, 1630009 (2016).
 - [4] Roberto Franzosi and Vittorio Penna, “Chaotic behavior, collective modes, and self-trapping in the dynamics of three coupled bose-einstein condensates,” *Physical Review E* **67**, 046227 (2003).
 - [5] A. R. Kolovsky and A. Buchleitner, “Quantum chaos in the bose-hubbard model,” *Europhysics Letters (EPL)* **68**, 632–638 (2004).
 - [6] S Mossmann and C Jung, “Semiclassical approach to bose-einstein condensates in a triple well potential,” *Physical Review A* **74**, 033601 (2006).
 - [7] Geva Arwas, Amichay Vardi, and Doron Cohen, “Superfluidity and chaos in low dimensional circuits,” *Scientific reports* **5**, 13433 (2015).
 - [8] Denis V Makarov and M Yu Uleysky, “Chaos-assisted formation of immiscible matter-wave solitons and self-stabilization in the binary discrete nonlinear schrödinger equation,” *Communications in Nonlinear Science and Numerical Simulation* **43**, 227–238 (2017).
 - [9] Christine Khripkov, Amichay Vardi, and Doron Cohen, “Many-body dynamical localization and thermalization,” *arXiv preprint arXiv:1908.03868* (2019).
 - [10] Roberto Franzosi, Vittorio Penna, and Riccardo Zecchina, “Quantum dynamics of coupled bosonic wells within the bose–hubbard picture,” *International Journal of Modern Physics B* **14**, 943–961 (2000).
 - [11] Michael Albiez, Rudolf Gati, Jonas Fölling, Stefan Hunsmann, Matteo Cristiani, and Markus K Oberthaler, “Direct observation of tunneling and nonlinear self-trapping in a single bosonic josephson junction,” *Physical review letters* **95**, 010402 (2005).
 - [12] R Gati and MK Oberthaler, “A bosonic josephson junction,” *Journal of Physics B: Atomic, Molecular and Optical Physics* **40**, R61 (2007).
 - [13] K Nemoto, CA Holmes, Gerard J Milburn, and WJ Munro, “Quantum dynamics of three coupled atomic bose-einstein condensates,” *Physical Review A* **63**, 013604 (2000).
 - [14] Roberto Franzosi and Vittorio Penna, “Self-trapping mechanisms in the dynamics of three coupled bose-einstein condensates,” *Physical Review A* **65**, 013601 (2001).
 - [15] Fernando M Cucchiatti, Horacio M Pastawski, and Rodolfo A Jalabert, “Universality of the lyapunov regime for the loschmidt echo,” *Physical Review B* **70**, 035311 (2004).
 - [16] Arseni Goussev, Rodolfo A Jalabert, Horacio M Pastawski, and Diego Ariel Wisniacki, “Loschmidt echo,” *Scholarpedia* **7**, 11687 (2012).
 - [17] Ya A Kharkov, VE Sotskov, AA Karazeev, EO Kiktenko, and AK Fedorov, “Revealing quantum chaos with machine learning,” *arXiv preprint arXiv:1902.09216* (2019).
 - [18] EM Graefe and HJ Korsch, “Semiclassical quantization of an n-particle bose-hubbard model,” *Physical Review A* **76**, 032116 (2007).
 - [19] J Esteve, C Gross, A Weller, S Giovanazzi, and MK Oberthaler, “Squeezing and entanglement in a bose–einstein condensate,” *Nature* **455**, 1216 (2008).
 - [20] Tilman Zibold, Eike Nicklas, Christian Gross, and Markus K Oberthaler, “Classical bifurcation at the transition from rabi to josephson dynamics,” *Physical review letters* **105**, 204101 (2010).
 - [21] AA Bychek, DN Maksimov, and AR Kolovsky, “Noon state of bose atoms in the double-well potential via an excited-state quantum phase transition,” *Physical Review A* **97**, 063624 (2018).

- [22] Augusto Smerzi and Andrea Trombettoni, “Nonlinear tight-binding approximation for bose-einstein condensates in a lattice,” *Physical Review A* **68**, 023613 (2003).
- [23] Andrey R Kolovsky, Hans Jürgen Korsch, and Eva-Maria Graefe, “Bloch oscillations of bose-einstein condensates: Quantum counterpart of dynamical instability,” *Physical Review A* **80**, 023617 (2009).
- [24] Zsolt Sándor, Bálint Érdi, András Széll, and Barbara Funk, “The relative lyapunov indicator: an efficient method of chaos detection,” *Celestial Mechanics and Dynamical Astronomy* **90**, 127–138 (2004).
- [25] SV Prants, M Edelman, and GM Zaslavsky, “Chaos and flights in the atom-photon interaction in cavity qed,” *Physical Review E* **66**, 046222 (2002).
- [26] Andrey R Kolovsky, “Semiclassical quantization of the bogoliubov spectrum,” *Physical review letters* **99**, 020401 (2007).
- [27] Andrey R Kolovsky and Dima L Shepelyansky, “Dynamical thermalization in isolated quantum dots and black holes,” *EPL (Europhysics Letters)* **117**, 10003 (2017).
- [28] Andrey R Kolovsky, “Microscopic models of source and sink for atomtronics,” *Physical Review A* **96**, 011601 (2017).
- [29] Fausto Borgonovi, Felix M Izrailev, Lea F Santos, and Vladimir G Zelevinsky, “Quantum chaos and thermalization in isolated systems of interacting particles,” *Physics Reports* **626**, 1–58 (2016).